



# Kent Academic Repository

Yang, Qingling, Gao, Steven, Luo, Qi, Wen, Lehu, Ban, Yong-Ling, Yang, Xuexia, Ren, Xiaofei and Wu, Jian (2019) *Dual-Polarized Crossed Slot Array Antenna Designed on a Single Laminate for Millimeter-Wave Applications*. IEEE Transactions on Antennas and Propagation, 68 (5). pp. 4120-4125. ISSN 0018-926X.

## Downloaded from

<https://kar.kent.ac.uk/78225/> The University of Kent's Academic Repository KAR

## The version of record is available from

<https://doi.org/10.1109/TAP.2019.2952244>

## This document version

Author's Accepted Manuscript

## DOI for this version

## Licence for this version

UNSPECIFIED

## Additional information

## Versions of research works

### Versions of Record

If this version is the version of record, it is the same as the published version available on the publisher's web site. Cite as the published version.

### Author Accepted Manuscripts

If this document is identified as the Author Accepted Manuscript it is the version after peer review but before type setting, copy editing or publisher branding. Cite as Surname, Initial. (Year) 'Title of article'. To be published in *Title of Journal*, Volume and issue numbers [peer-reviewed accepted version]. Available at: DOI or URL (Accessed: date).

## Enquiries

If you have questions about this document contact [ResearchSupport@kent.ac.uk](mailto:ResearchSupport@kent.ac.uk). Please include the URL of the record in KAR. If you believe that your, or a third party's rights have been compromised through this document please see our [Take Down policy](https://www.kent.ac.uk/guides/kar-the-kent-academic-repository#policies) (available from <https://www.kent.ac.uk/guides/kar-the-kent-academic-repository#policies>).

# Communication

## Dual-Polarized Crossed Slot Array Antenna Designed on a Single Laminate for Millimeter-Wave Applications

Qingling Yang, *Student Member, IEEE*, Steven Gao, *Fellow, IEEE*, Qi Luo, *Senior Member, IEEE*, Lehu Wen, Yong-Ling Ban, Xuexia Yang, *Senior Member, IEEE*, Xiaofei Ren, and Jian Wu

**Abstract**—A novel dual-polarized crossed slot planar array antenna is presented in this paper. The proposed design integrates the antenna array with the feeding networks on a single laminate. The antenna element is developed by using a  $TE_{210}$  and  $TE_{120}$  mode cavity, which is constructed by inserting a number of metalized posts around the crossed region of two perpendicular substrate integrated waveguides (SIWs). The crossed slot is etched over the cavity and is excited from two orthogonal directions to realize dual-polarization. Owing to the orthogonality between the  $TE_{210}$  and  $TE_{120}$  mode, high isolation and low cross-polarization are achieved. A prototype of the designed antenna array operating at 25 GHz is fabricated and measured. The measured results confirm that the presented array antenna has high port isolation ( $> 41$  dB), high cross-polarization discrimination (XPD) ( $> 26$  dB) and high aperture efficiency (40%). With advantages of simple configuration, good radiation performance and easy fabrication, this proposed array antenna is a good candidate for millimeter-wave wireless systems.

**Index Terms**—Dual-polarized antenna, planar array, SIW cavity, slot antenna

### I. INTRODUCTION

Dual-polarized antennas are highly desirable in modern wireless systems since they can combat multi-path fading and improve channel capacity [1]. In recent years, millimeter waves (mmWaves) wireless systems have received many interests with benefits such as large bandwidth, high resolution and small size [2]. However, it is challenging to realize dual-polarized antenna arrays working in mmWave frequency bands. One of the key constraints is that there are limited types of dual-polarized antennas suitable for integrating with feeding networks [3]–[17]. For instance, although the microstrip antenna reported in [3] operates with dual-polarization, it is only used to design a linear array. This is because the feeding networks are interleaved with the antenna elements so that grating lobes will appear if a planar antenna array is realized by using this antenna element. In addition, dual-polarized mmWave antenna arrays with a large number of elements are very intricate as each polarization requires an independent feeding network. The slot antenna arrays reported in [10] and

[11] can provide dual-polarization while being integrated with the feeding networks on a single laminate, but the orthogonally polarized antenna elements in these antenna arrays are separated in different rows. As a result, these antenna arrays have a relatively large aperture size and high cross-polarization level. Thus, in order to achieve high compactness and avoid intersections between feeding networks, many dual-polarized antenna arrays are realized by using multiple laminates [12]–[16]. However, compared with the antenna arrays designed on a single laminate, these antenna arrays have higher design complexity and insertion loss. Besides, the milling technique is used to fabricate the dual-polarized array antennas [14]–[16], yet the fabricated antenna prototypes are bulky and expensive.

The objective of this work is to design a dual-polarized array antenna with simple geometry and good performance. We develop a novel planar dual-polarized crossed slot frequency-scanning antenna array that can be integrated with the feeding networks on a single laminate. An SIW cavity supporting  $TE_{210}$  and  $TE_{120}$  modes is employed in designing the antenna element. Different from the conventional  $TE_{210}$  or  $TE_{120}$  mode cavities shaped by metalized walls with a closed form [18], [19], this cavity is constructed by inserting a number of metalized posts around the crossed region of two perpendicular SIWs. The crossed slot etched over the cavity is excited from orthogonal directions to generate dual-polarization. High port isolation, high aperture efficiency and high XPD are obtained in the designed antenna array. Furthermore, the antenna has three additional advantages: 1) it is realized on a single laminate with low cost; 2) it is scalable; 3) it is highly compact and can be easily integrated with front ends.

### II. GEOMETRY OF THE ANTENNA ARRAY

The layout of the proposed dual-polarized array antenna is illustrated in Fig. 1. In this design, Rogers RT/duroid 5880 laminate with thickness of 0.508 mm,  $\epsilon_r = 2.2$  and  $\tan \delta = 0.0009$  is used. The antenna array aperture consists of  $10 \times 10$  dual-polarized antenna elements. Four feeding ports with SIW-to-GCPW (grounded co-planar waveguide) transitions connected to a ten-way equal splitter are used to excite the antenna array. Since each antenna element has high isolation between two orthogonal ports, the full planar array antenna can be considered as ten linear antenna arrays placed in parallel. The number of antenna elements in each column and row is set to  $n = 10$ . The total radiated power  $P_{rad}$  for each linear array is assumed to be  $0.95P_0$ , where  $P_0$  is the input power. The radiation efficiency of each antenna

This work was funded by China Research Institute of Radiowave Propagation, EPSRC under grants EP/P015840/1, EP/N032497/1 and EP/S005625/1. (Corresponding author: Qingling Yang)

Q. Yang, S. Gao, Q. Luo and L. Wen are with the School of Engineering and Digital Arts, University of Kent, Canterbury CT2 7NZ, UK.

Y. Ban is with the School of Electronic Science and Engineering, University of Electronic Science and Technology of China, Chengdu 611731, China.

X. Yang is with the School of Communication and Information Engineering, Shanghai University, Shanghai 200444, China.

X. Ren and J. Wu are with the China Research Institute of Radiowave Propagation, Xinxiang, Henan 453003, China.

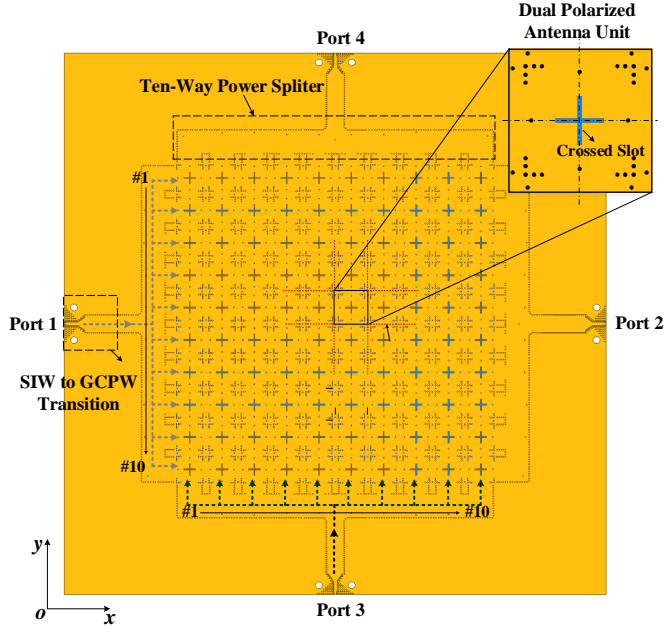


Fig. 1. Layout of the proposed dual-polarized crossed slot planar antenna array.

element is assumed to be  $\eta$ . Thus, the radiation power  $P_{i\_rad}$  ( $i = 1, 2, \dots, n$ ) of the  $i$ th antenna element in each column or row is

$$P_{i\_rad} = \eta(1 - \eta)^{i-1} P_0 \quad (1)$$

Therefore, the radiated power  $P_{rad}$  of each linear antenna array is

$$P_{rad} = \sum_{i=1}^n P_{i\_rad} = \sum_{i=1}^n \eta(1 - \eta)^{i-1} P_0 = 0.95P_0 \quad (2)$$

By solving (2), the desired radiation efficiency of each antenna element is calculated to be 26%. In our design, the antenna element can be regarded as a four-port network. Thus the radiation efficiency of each element is obtained from the  $S$ -parameters of the four-port network [4], which is expressed as:

$$\eta = \frac{1 - |S_{11}|^2 - |S_{21}|^2 - |S_{31}|^2 - |S_{41}|^2}{1 - |S_{11}|^2} \times 100\% \quad (3)$$

In this formula, the ohmic losses are not taken into account. Be noted that the dielectric losses are included in (3), because the  $S$ -parameters are obtained from the HFSS simulations where the dielectric losses of Rogers RT/duroid 5880 laminate are considered.

### III. ANTENNA ELEMENT AND ANTENNA ARRAY DESIGN

#### A. Dual-Polarized Antenna Element

Fig. 2 shows the configuration of the developed dual-polarized antenna element. It consists of a crossed slot over a cavity supporting  $TE_{210}$  and  $TE_{120}$  modes. The cavity is formed by a number of metalized posts. Four of these posts are located along the center line and the rest are placed around

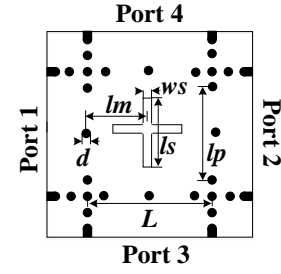


Fig. 2. Layout of the antenna element. Detailed dimensions are  $l_m = 3.48$  mm,  $d = 0.3$  mm,  $w_s = 0.3$  mm,  $l_s = 3$  mm,  $l_p = 5$  mm, and  $L = 7$  mm.

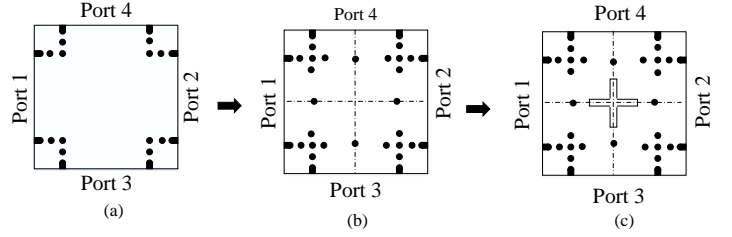


Fig. 3. Design process of the antenna element. (a) Two perpendicular SIWs. (b)  $TE_{210}$  and  $TE_{120}$  mode cavity. (c) Proposed antenna element.

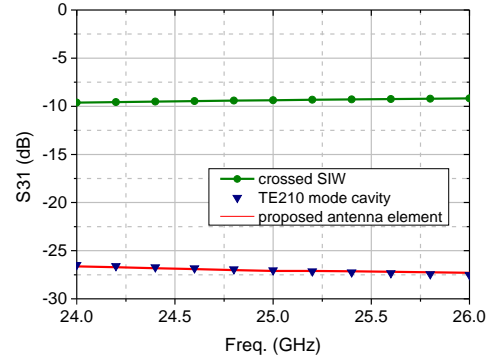


Fig. 4. Simulated  $S_{31}$  for three different structures.

the corners. The dominant frequency  $f_0$  in a square  $TE_{210}$  or  $TE_{120}$  mode cavity is [20]:

$$f_0 \approx \frac{\sqrt{5}c_0}{2L\sqrt{\epsilon_r}} \quad (4)$$

where  $c_0$  is the velocity of waves traveling in free-space,  $\epsilon_r$  is the relative permittivity of the laminate and  $L$  is the side length of the square cavity. It is worth mentioning that (4) is exact for fully enclosed cavity. Therefore, the synthesized cavity size  $L$  should be smaller than the theoretical one. The proposed antenna element operates with horizontal polarization by exciting Port 1 or Port 2 and in this case Port 3 and Port 4 are isolated. Vertical polarization is achieved by exciting Port 3 or Port 4, while Port 1 and Port 2 are isolated correspondingly.

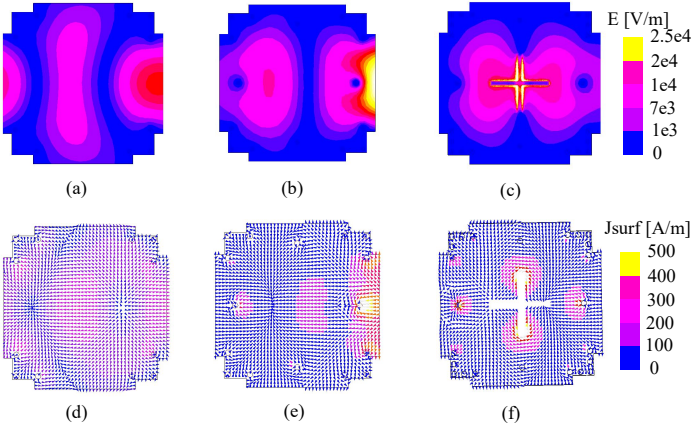


Fig. 5. Field and current distribution. (a)–(c) Electric field distribution in the structures presented in Fig. 3(a), (c) and (d) respectively. (d)–(f) Current distribution in the structures presented in Fig. 3 (a), (c) and (d) respectively.

### B. Antenna Design

To illustrate the design process of the proposed antenna element, the reference structures are shown in Fig. 3. As shown in Fig. 3(a), the proposed antenna is developed from a crossed SIW where two SIWs are perpendicular to each other with an open region. In Fig. 3(b), a number of metalized posts are inserted around the crossed region to form a  $TE_{210}$  and  $TE_{120}$  mode cavity. Four of these metalized posts are placed along the centerlines, and the rest of them are located around the corners. As shown in Fig. 3(c), the proposed antenna is realized by etching a crossed slot over the cavity. Fig. 4 shows the simulated  $S_{31}$  of the reference structures in the design process. In the crossed SIW, strong coupling higher than  $-10$  dB in the band 24 GHz–26 GHz is observed between Port 1 and Port 3. The isolation is improved by exciting the  $TE_{210}$  and  $TE_{120}$  mode of the SIW cavity, which is higher than 26 dB. Thus, the crossed slot etched over the cavity can be excited from two orthogonal directions to realize dual-polarization while maintaining high isolation.

In the proposed antenna, high isolation and high XPD are achieved by the orthogonality between  $TE_{210}$  and  $TE_{120}$  mode. In order to better illustrate the working principle of the proposed dual-polarized antenna, the field distribution in the reference structures are shown in Fig. 5. From Fig. 5(a), it is observed that the field is distributed at Port 3 and Port 4 when Port 1 is excited. This is because no structures are applied to constrain the field behavior in the open region of the crossed SIW. In the SIW cavity, most of the electric fields are restrained to propagate along the horizontal direction, as shown in Fig. 5(b). However, it should be noted that the  $TE_{210}$  mode field distribution in the SIW cavity are not odd symmetric. It results in degraded polarization purity if a slot antenna is designed with such a cavity. To address this issue, it is necessary to introduce an additional perturbation into the cavity. As shown in Fig. 5(c), the presence of the crossed slot affects the electric field distribution inside the cavity. Thus, the crossed slot in this structure acts not only as a dual-polarized radiating element but also a perturbation to improve the symmetry of the  $TE_{210}$  mode. In this cavity, the electric

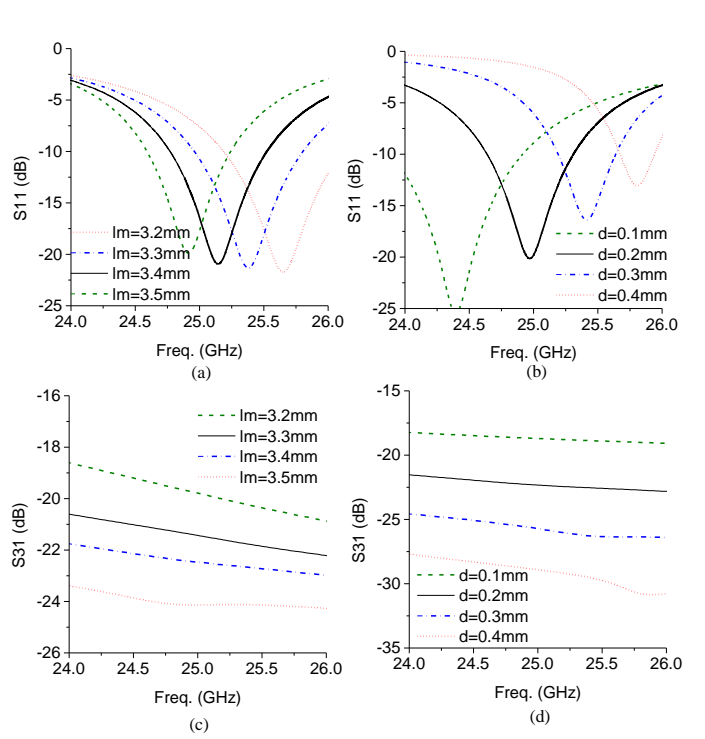


Fig. 6. Parametric study of the effect of different geometrical parameters on the  $S$  parameters. Effects of (a)  $l_m$  and (b)  $d$  on the  $S_{11}$  and effect of (c)  $l_m$  and (d)  $d$  on the  $S_{31}$ .

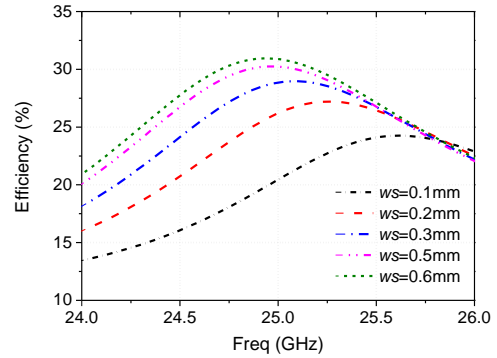


Fig. 7. Effect of  $w_s$  on the radiation efficiency.

fields of the  $TE_{210}$  mode have equal magnitude but are out of phase across the center line. The waves are well restrained to propagate along the horizontal direction. When Port 1 is excited, the transverse slot is excited to radiate horizontally polarized waves, because the electric fields on both sides of the transverse slot are out of phase. In addition, as can be seen from Fig. 5(c) and (f), almost no fields are observed at Port 3 and Port 4, indicating that high port isolation is achieved. Similarly, the  $TE_{120}$  mode is observed in the cavity when either Port 3 or Port 4 is excited. In this case, the longitudinal slot of this antenna element is excited and radiate vertically polarized waves, while the horizontal ports (Port 1 and Port 2) are well isolated.

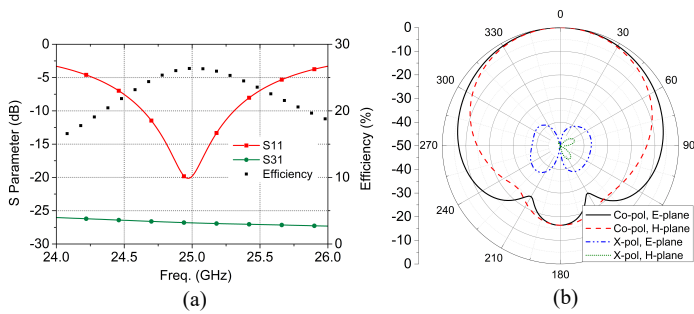


Fig. 8. Simulated performance of the proposed antenna element. (a)  $S$ -parameters and radiation efficiency. (b) Normalized radiation patterns.

For the proposed antenna element, the resonance of the antenna element and the isolation between Port 1 and Port 3 (or Port 4) are mainly affected by the location ( $l_m$ ) and size ( $d$ ) of the inserted posts at the center lines. As shown in Fig. 6(a), by increasing  $l_m$ , the resonant frequency shifts to the lower frequency band, because the effective cavity size is enlarged. The small variation of the reflection coefficients for different  $l_m$  indicates that the location of the metalized posts at the center lines mainly affect the resonance while the return loss remains stable at the resonant frequencies. In Fig. 6(b), it is shown that the resonant frequency of the cavity is sensitive to the size of the metalized posts. The resonant frequency is increased by enlarging the post size. As shown in Fig. 6(c) and (d), high port isolation is obtained by increasing  $l_m$  and decreasing the size of the inserted metalized posts. The radiation efficiency of the proposed antenna can be tuned by varying the slot width  $w_s$ , as shown in Fig. 7. When  $w_s$  is increased, the peak efficiency shifts to the lower frequency and is increased.

### C. Antenna Element Performance

The optimized dimensions of the developed antenna element are shown in the caption of Fig. 2. Fig. 8(a) shows the simulated  $S$ -parameters and radiation efficiency of the designed antenna element. High return loss and high port isolation are achieved. The  $-10$  dB reflection coefficient bandwidth is 700 MHz (24.6 GHz–25.3 GHz) and the isolation between Port 1 and Port 3 is higher than 26 dB. The radiation efficiency is 26.3% at the center frequency, which is close to the desired radiation efficiency calculated from (2). Fig. 8(b) presents the simulated radiation patterns of the antenna element at 25 GHz. Symmetrical patterns are observed in both  $E$ -plane and  $H$ -plane. In addition, the XPD is higher than 40 dB. This demonstrates that good dual-polarized radiation is realized in the designed antenna element.

### D. Subarray

Using the developed antenna element, a subarray composed of two linear antenna arrays is designed and shown in Fig. 9(a). The antenna element spacing is 9.4 mm, which is  $0.78\lambda_0$  at 25 GHz. In this subarray, Port 1 and Port 2 are simultaneously excited with uniform amplitude and phase. Port A1–A10 and Port B1–B10 are connected to the subsequent linear arrays. All these ports including Port 3 and Port 4 are

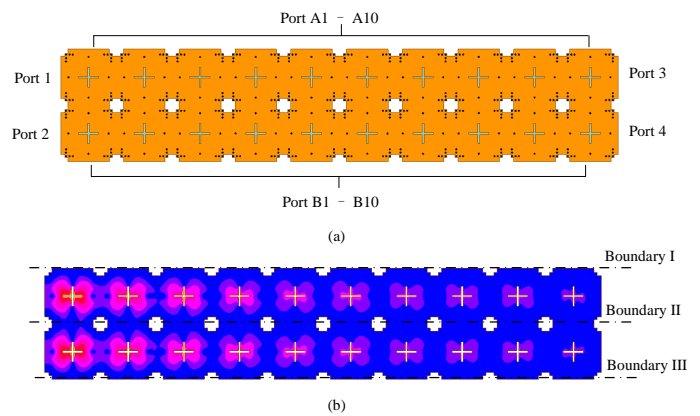


Fig. 9. Subarray formed by two linear antenna arrays. (a) Geometry. (b) Field distribution when Port 1 and Port 2 are excited synchronously.

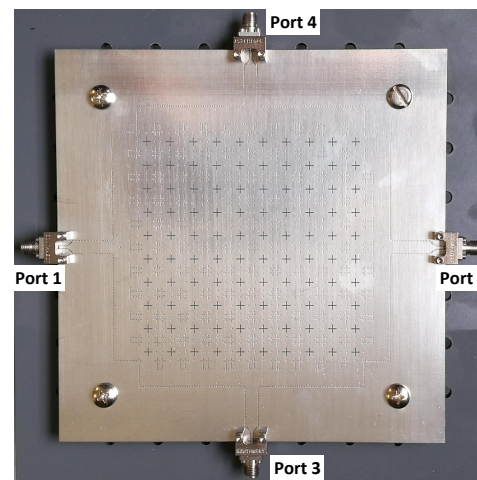


Fig. 10. Fabricated prototype of the array antenna.

terminated with a matched load. Fig. 9(b) shows the simulated electric field distribution of the subarray at 25 GHz. It is observed that at Boundary I, Boundary I, and Boundary III the fields are reduced to a very weak level. This indicates that the waves in the two linear arrays are bounded by three virtual SIWs. Signals are allowed to independently travel in the two linear arrays with little interference. The electric fields in the substrate are gradually radiated and decayed along each linear array. Similar field distribution can be observed when excitation is from the vertical direction. Thus, the planar antenna array composed of the proposed antenna element is scalable and can be excited from different directions to realize dual-polarization on a single laminate.

## IV. MEASUREMENT AND DISCUSSION

A prototype of the presented dual-polarized antenna array was fabricated and shown in Fig. 10. Its dimension is 157.4 mm  $\times$  157.4 mm  $\times$  0.508 mm and the antenna array aperture size is 94 mm  $\times$  94 mm. Four 2.92 mm end-launch connectors are used to connect the antenna with test equipment. The screws are used to fix the fabricated antenna to the test platform.

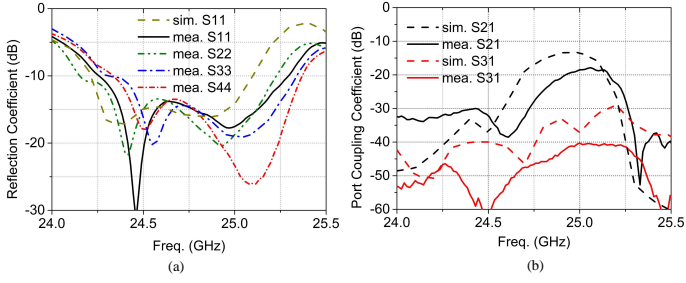


Fig. 11. Simulated and measured  $S$ -parameters of the fabricated array antenna. (a) Reflection coefficient. (b) Port coupling level.

### A. Return Loss and Isolation

Fig. 11 shows the measured and simulated  $S$ -parameters of the fabricated prototype. The measured  $S_{11}$  agrees well with the simulated results, as shown in Fig. 11(a). The measured reflection coefficient  $S_{11}$  less than  $-10$  dB is from 24.2 GHz to 25.35 GHz. Due to the symmetry of the antenna array, the reflection coefficient at each port is very similar. The overlapped bandwidth for which all the ports are matched below  $-10$  dB is 24.3 GHz–25.25 GHz.

The measured and simulated port isolations are shown in Fig. 11(b). The simulated  $S_{21}$  is  $-13$  dB which is very close to the designed residual power,  $0.05P_0$ . Within the bandwidth, the measured transmission loss between Port 1 and Port 2 is lower than the simulated one due to additional loss caused by the connectors. The simulated isolation between Port 1 and Port 3 is larger than 30 dB within the bandwidth, while the measured one is higher than 41 dB.

### B. Radiation Pattern

Fig. 12 shows the comparison between the simulated and measured normalized radiation patterns at 24.8 GHz, 25 GHz and 25.2 GHz when Port 1 and Port 2 are excited. A good agreement between the simulated and measured results is achieved. The frequency scanning radiation patterns are shown in Fig. 12(a). From 24.8 GHz to 25.2 GHz, a scanning range of  $36^\circ$  is realized, where the beams from  $-18^\circ$  to  $0^\circ$  are realized by frequency scanning with Port 1 excited, and scanning range from  $0^\circ$  to  $18^\circ$  are realized with Port 2 excited. The side lobe levels are less than  $-9.3$  dB over the frequency bandwidth. The  $-3$  dB beamwidth at different frequencies keeps stable, which is with an average of  $8^\circ$ . The overlapped levels between radiation patterns are higher than  $-2.9$  dB. As shown in Fig. 12(b), the cross-polarization keeps in a low level because of high polarization purity and high port isolation in the antenna element. The measured XPD at 25 GHz is larger than 26 dB.

### C. Gain and Efficiency

Fig. 13 shows the simulated and measured gain and efficiency of the designed planar array antenna. It shows that the antenna has a high gain from 24.6 GHz–25.3 GHz. The simulated realized gain is up to 25.7 dBi with a variation of 2.8 dB over the bandwidth. In comparison, the measured gains

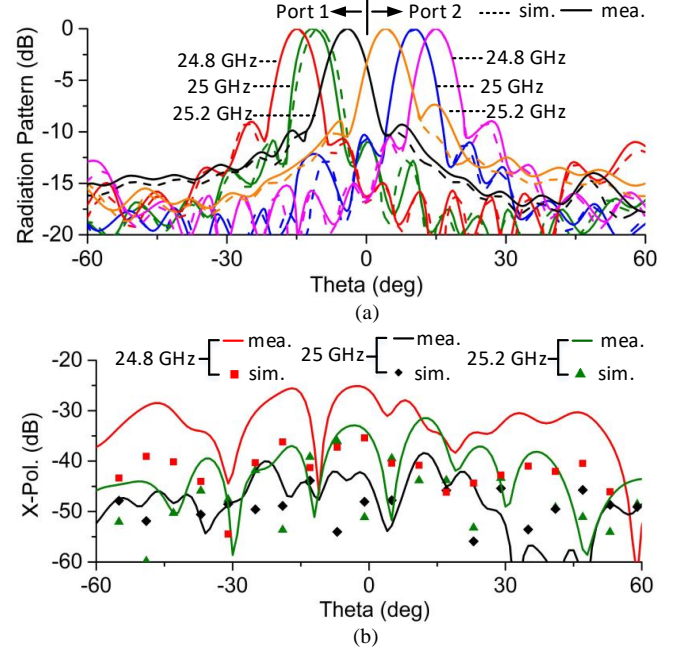


Fig. 12. Radiation patterns. (a) Simulated and measured co-polarization patterns. (b) Simulated and measured XPD patterns.

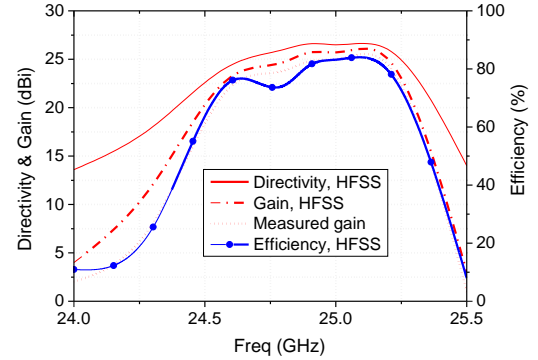


Fig. 13. Directivity, gain and radiation efficiency.

are about 0.8 dB lower than the simulated ones over the bandwidth. This discrepancy is caused by the connector insertion loss, fabrication tolerance and uncertainty of dielectric loss. The measured gain has a peak value of 24.9 dBi. The radiation efficiency is larger than 76% from 24.6 GHz–25.3 GHz, which is calculated from the simulated directivity and gain.

### D. Comparison

A comparison between this work and the recently reported frequency-scanning antenna arrays is summarized in Table I. The antenna array in [4] is a dual-polarized frequency-scanning array antenna with high XPD. However, it has a narrow frequency-scanning range and low aperture efficiency. Although the antenna arrays in [5] and [10] provide dual-polarization while being implemented on a single laminate,

TABLE I  
COMPARISON BETWEEN THIS WORK AND THE REPORTED  
FREQUENCY-SCANNING ARRAY ANTENNAS

Ref.	BW (GHz)	No. Sub.	Scanning Range	Pol.	XPD (dB)	Array Type	$\eta_{ap}$
[4]	2.7-3.0	3	(70°,88°)	dual	30	linear	14%
[5]	2.4-2.48	1	n.a.	dual	16	planar	11%
[10]	33-39	1	(1°,35°)	dual	18	linear	34%
[21]	8.5-14.1	3	(-17°,52°)	single	n.a.	linear	34%
[22]	8.9-10.6	3	(-28°,46°)	single	n.a.	linear	20%
[23]	13.5-13.9	1	(2°,37°)	single	n.a.	linear	17%
[24]	28-32	2	(4°,20°)	single	27	linear	28%
Proposed	24.8-25.2	1	(-18°,18°)	dual	26	planar	40%

they are realized by designing the orthogonal antenna elements in separate rows. Hence, the cross-polarization level of these antennas is degraded and their aperture efficiency is limited to 34%. The antenna arrays in [21] and [22] have wide scanning range, but they are limited to single polarization and are difficult to be used in planar arrays. In addition, multiple substrates are needed to realize such array antennas. The antenna arrays in [23] and [24] only provide single polarization and have limited scanning range. As can be seen from the table, although the proposed antenna array has a relatively narrow impedance bandwidth, it is dual-polarized and can be realized on a single laminate. The frequency scanning range of the proposed antenna array is from  $-18^\circ$  to  $18^\circ$ . Besides, it also has advantages of high aperture efficiency (40%) and high XPD ( $>26$  dB) as compared with other reported frequency-scanning array antennas.

## V. CONCLUSION

A planar dual-polarized crossed slot array antenna based on a SIW cavity supporting  $TE_{210}$  and  $TE_{120}$  modes is presented. The antenna array is realized on a single laminate with simple configuration, high integration and low profile. The  $10 \times 10$  antenna array operating at 25 GHz is fabricated and measured. The measured port isolation is higher than 41 dB. The measured peak gain is 24.9 dBi and the measured XPD is higher than 26 dB. The aperture efficiency of this array antenna is 40%. The simulated radiation efficiency is higher than 76% within the operation bandwidth. The presented array antenna can be easily integrated with the front ends. Thus, it is a good candidate for wireless communication systems.

## REFERENCES

[1] V. Eiceg, H. Sampath and S. Catreux-Erceg, "Dual-polarization versus single-polarization MIMO channel measurement results and modeling," *IEEE Trans. Wireless Commun.*, vol. 5, no. 1, pp. 28-33, Jan. 2006.

[2] D. Liu, W. Hong, T. S. Rappaport, C. Luxey and W. Hong, "What will 5G Antennas and Propagation Be?," *IEEE Trans. Antennas and Propag.*, vol. 65, no. 12, pp. 6205-6212, Dec. 2017.

[3] G. F. Hamberger, S. Trummer, U. Siart and T. F. Eibert, "A planar dual-polarized microstrip 1-D-beamforming antenna array for the 24-GHz band," *IEEE Trans. Antennas and Propag.*, vol. 65, no. 1, pp. 142-149, Jan. 2017.

[4] S. Karimkashi and G. Zhang, "A Dual-Polarized Series-Fed Microstrip Antenna Array With Very High Polarization Purity for Weather Measurements," *IEEE Trans. Antennas and Propag.*, vol. 61, no. 10, pp. 5315-5319, Oct. 2013.

[5] Y. Li, Z. Zhang, C. Deng, Z. Feng and M. F. Iskander, "2-D Planar Scalable Dual-Polarized Series-Fed Slot Antenna Array Using Single Substrate," *IEEE Trans. Antennas and Propag.*, vol. 62, no. 4, pp. 2280-2283, April 2014.

[6] Y. Li and K. Luk, "60-GHz dual-polarized two-dimensional switch-beam wideband antenna array of aperture-coupled magneto-electric dipoles," *IEEE Trans. Antennas and Propag.*, vol. 64, no. 2, pp. 554-563, Feb. 2016.

[7] A. Li, K. Luk and Y. Li, "A dual linearly polarized end-fire antenna array for the 5G applications," *IEEE Access*, vol. 6, pp. 78276-78285, 2018.

[8] L. Schulwitz and A. Mortazawi, "Millimeter-wave dual polarized L-shaped horn antenna for wide-angle phased arrays," *IEEE Trans. Antennas and Propag.*, vol. 54, no. 9, pp. 2663-2668, Sept. 2006.

[9] M. Esquius-Morote, M. Mattes and J. R. Mosig, "Orthomode transducer and dual-polarized horn antenna in substrate integrated technology," *IEEE Trans. Antennas and Propag.*, vol. 62, no. 10, pp. 4935-4944, Oct. 2014.

[10] Y. J. Cheng, W. Hong and K. Wu, "Millimeter-Wave Half Mode Substrate Integrated Waveguide Frequency Scanning Antenna With Quadri-Polarization," *IEEE Trans. Antennas and Propag.*, vol. 58, no. 6, pp. 1848-1855, June 2010.

[11] Sehyun Park, Y. Okajima, J. Hirokawa and M. Ando, "A slotted postwall waveguide array with interdigital structure for  $45^\circ$  linear and dual polarization," *IEEE Trans. Antennas and Propag.*, vol. 53, no. 9, pp. 2865-2871, Sept. 2005.

[12] J. Xu, W. Hong, Z. H. Jiang, J. Chen and H. Zhang, "A Q-Band Low-Profile Dual Circularly Polarized Array Antenna Incorporating Linearly Polarized Substrate Integrated Waveguide-Fed Patch Subarrays," *IEEE Trans. Antennas and Propag.*, vol. 65, no. 10, pp. 5200-5210, Oct. 2017.

[13] Z. Chen, H. Liu, J. Yu and X. Chen, "High gain, broadband and dual-polarized substrate integrated waveguide cavity-backed slot antenna array for 60 GHz band," *IEEE Access*, vol. 6, pp. 31012-31022, 2018.

[14] G. Huang, S. Zhou, T. Chio, C. Sim and T. Yeo, "Waveguide-stripline seriescorporate hybrid feed technique for dual-polarized antenna array applications," *IEEE Trans. Compon. Packag. Manuf. Technol.*, vol. 7, no. 1, pp. 81-87, Jan. 2017.

[15] X. Lu, H. Zhang, S. Gu, H. Liu, X. Wang and W. Lu, "A dual-polarized cross-slot antenna array on a parallel-plate waveguide with compact structure and high efficiency," *IEEE Antennas Wirel. Propag. Lett.*, vol. 17, no. 1, pp. 8-11, Jan. 2018.

[16] D. Kim, M. Zhang, J. Hirokawa and M. Ando, "Design and fabrication of a dual-polarization waveguide slot array antenna with high isolation and high antenna efficiency for the 60 GHz band," *IEEE Trans. Antennas and Propag.*, vol. 62, no. 6, pp. 3019-3027, June 2014.

[17] H. Chu and Y. Guo, "A filtering dual-polarized antenna subarray targeting for base stations in millimeter-wave 5G wireless communications," *IEEE Trans. Compon. Packag. Manuf. Technol.*, vol. 7, no. 6, pp. 964-973, June 2017.

[18] J. Xu, Z. N. Chen, X. Qing and W. Hong, "140-GHz  $TE_{20}$ -mode dielectric-loaded SIW slot antenna array in LTCC," *IEEE Trans. Antennas and Propag.*, vol. 61, no. 4, pp. 1784-1793, April 2013.

[19] S. A. Winkler, W. Hong, M. Bozzi and K. Wu, "Polarization rotating frequency selective surface based on substrate integrated waveguide technology," *IEEE Trans. Antennas and Propag.*, vol. 58, no. 4, pp. 1202-1213, April 2010.

[20] Y. Wu, Y. Chen, L. Jiao, Y. Liu and Z. Ghassemlooy, "Dual-band dual-mode substrate integrated waveguide filters with independently reconfigurable  $TE_{101}$  resonant mode," *Sci. Rep.*, pp. 31922, Aug. 2016.

[21] X. Yang, L. Di, Y. Yu and S. Gao, "Low-Profile Frequency-Scanned Antenna Based on Substrate Integrated Waveguide," *IEEE Trans. Antennas and Propag.*, vol. 65, no. 4, pp. 2051-2056, April 2017.

[22] L. Cui, W. Wu and D. Fang, "Printed Frequency Beam-Scanning Antenna With Flat Gain and Low Sidelobe Levels," *IEEE Antennas Wirel. Propag. Lett.*, vol. 12, pp. 292-295, 2013.

[23] D. Guan, Q. Zhang, P. You, Z. Yang, Y. Zhou and S. Yong, "Scanning Rate Enhancement of Leaky-Wave Antennas Using Slow-Wave Substrate Integrated Waveguide Structure," *IEEE Trans. Antennas and Propag.*, vol. 66, no. 7, pp. 3747-3751, July 2018.

[24] K. Mak, K. So, H. Lai and K. Luk, "A Magnetolectric Dipole Leaky-Wave Antenna for Millimeter-Wave Application," *IEEE Trans. Antennas and Propag.*, vol. 65, no. 12, pp. 6395-6402, Dec. 2017.